HHS Public Access

Author manuscript

Cancer Lett. Author manuscript; available in PMC 2016 August 28.

Published in final edited form as:

Cancer Lett. 2015 August 28; 365(1): 89–95. doi:10.1016/j.canlet.2015.05.019.

Three–dimensional (3D) culture of bone–derived human 786–O renal cell carcinoma retains relevant clinical characteristics of bone metastases

Tianhong Pan[a], **Eliza L.S. Fong**[b], **Mariane Martinez**[c], **Daniel A. Harrington**[c], **Sue-Hwa Lin**[d], **Mary C. Farach-Carson**[b,c], and **Robert L. Satcher**[a,*]

[a]Department of Orthopaedic Oncology, The University of Texas MD Anderson Cancer Center, Houston, TX, USA

[b]Department of Bioengineering, Rice University, Houston, TX, USA

[c]Department of BioSciences, Rice University, Houston, TX, USA

[d]Department of Translational Molecular Pathology, The University of Texas MD Anderson Cancer Center, Houston, TX USA

Abstract

Bone metastases from renal cell carcinoma (RCC) are typically lytic, destructive, and resistant to treatment regimens. Current *in vitro* models for studying metastasis introduce artifacts that limit their usefulness. Many features of tumors growing in bone are lost when human RCC cells are cultured in two-dimensional (2D) plastic substrata. In this study, we established that RCC spheroids, consisting of aggregates of cells, can be grown in a three-dimensional (3D) hyaluronate hydrogel-based culture system. The bone-derived human 786-O RCC subline proliferated and survived long term in these hydrogels. Additionally, RCC spheroids in 3D hydrogels demonstrated lower proliferation rates than their counterparts grown in 2D. Overall, gene expression patterns of RCC spheroids in 3D more closely mimicked those observed *in vivo* than did those of cells grown in 2D. Of particular importance, selected adhesion molecules, angiogenesis factors and osteolytic factors that have been shown to be involved in RCC bone metastasis were found to be expressed at higher levels in 3D than in 2D cultures. We propose that the 3D culture system provides an improved platform for RCC bone metastasis studies compared with 2D systems.

Keywords

Bone metastasis; Hyaluronic acid; Hydrogel; Renal cell carcinoma; Three dimensional culture

[*]Corresponding author. Tel.: +1 713 794 5242; fax: +1 713 792 8448. rlsatcher@mdanderson.org (R.L. Satcher).

Conflict of interest

None.

Introduction

As the 10th leading cause of cancer death, the morbidity and mortality of renal cell carcinoma (RCC) are largely attributed to its tendency to metastasize in an organ-specific manner [1-3]. One of the common sites of RCC metastasis is bone, where resulting lesions are typically painful, lytic, destructive, and difficult to treat [4,5]. To develop more effective therapies, we must better understand the key RCC survival and growth mechanisms that cause bone metastases.

Recent studies have shown that fundamental understanding of cancer metastasis is not readily obtained using 2D cell culture [6,7]. The standard plastic substrate does not create the complex and dynamic cell–cell and cell–matrix interactions that occur during cancer metastasis. In addition, the spatial cues, including depth and cell connectivity, limit the applicability of 2D culture to accurately test pharmacologically active compounds. Accordingly, 3D tumor models have been developed to more accurately reproduce the feature of native tumor and metastasis microenvironments [6,8-10]. In particular, several groups have reported on 3D models of prostate cancer (PCa) [11-15]. However, in our review of the literature, we were unable to identify 3D models of RCC.

In this study, we report the development of a 3D *in vitro* culture system for RCC bone metastasis tumoroids. We hypothesized that if 3D models are to replace conventional 2D cultures, cancer cells grown in them should adopt a phenotype and express biomarkers that mimic the tumors *in vivo*. This includes tumoroid expression of markers associated with cell–cell contact in 3D, such as adhesion complexes, which provide survival signals and drug resistance. Additionally, as RCC bone metastases are both highly vascularized and lytic, cells in 3D should express those molecules known to activate nearby endothelial cells and osteoclastic precursors.

3D hydrogels composed of hyaluronan or modified hyaluronan have been previously shown to support the long term growth of bone metastatic PCa cells, including those from patient-derived xenografts [13-16]. In this study, we examined whether 3D cultures of the human 786-O RCC subline derived from bone metastases in HA-based hydrogel would provide a useful model for studying treatment resistance in RCC.

Material and methods

Cell culture and preparation of cell-laden hydrogel constructs

Bone-derived 786-O RCC cells (bone-786-O RCC) used in this study were generated from bone metastases using an *in vivo* metastatic model established by intra-cardially injecting severe combined immune-deficient (SCID) mice with human 786-O RCC cells that were expressing luciferase (Luc) and green fluorescent protein (GFP) (Fig. 1) [17]. Bone-786-O RCC cells were cultured at 37 °C with 5% CO_2 in RPMI medium (Invitrogen) supplemented with 10% (v/v) fetal bovine serum (FBS). Thiol-modified HA (HA-SH, Glycosil, average M_w = 240 kDa, degree of thiolation = 1 μmol/mg HA-SH) and poly(ethylene glycol)-diacrylate (PEG-DA, Extralink, average M_w = 3350 Da) were obtained from BioTime Inc. (Alameda, CA). The procedure for encapsulating cells was employed as per the

manufacturer's instructions. Specifically, hydrogel constructs were fabricated as a bilayer, with a cell-laden upper layer above an acellular bottom layer. To prepare the bottom layer, PEG-DA was mixed with HA-SH in the volume ratio 1:4 to a total volume of 25 μL and pipetted into custom-made molds as we previously described [13]. After 10 min, the upper cell-laden layer, prepared by mixing a pellet of 1×10^5 cells with HA-SH followed by the addition of PEG-DA at the same volume ratio as the bottom layer, was layered above the bottom layer. The hydrogel constructs were then incubated at 37 °C for 30 min to allow for polymerization. Complete medium was then added to fully submerge the hydrogel constructs and incubated overnight. The next day, the hydrogel constructs were transferred to wells of 48-well plates containing 500 μl of complete medium in each well. Culture medium was changed every other day.

Cell viability and growth

The PrestoBlue reagent kit (Life Technologies, Grand Island, NY) was used to measure cell viability overtime. For 2D culture, 2×10^4 cells were seeded into each well of a 96-well plate containing 200 μl of culture medium and cell viability was determined at days 1, 2, 3 and 4. For 3D culture, each hydrogel construct encapsulating 1×10^5 cells was cultured in 48-well plates containing 500 μl of culture medium and cell viability was determined at days 1, 8, 16 and 24. At each time-point, medium in each well was exchanged with 100 μl (for 2D) or 350 μl (for 3D) of fresh medium. PrestoBlue reagent was added to each well at a 1:10 (v/v) ratio, and cells were further incubated at 37 °C for 2 h. Then 100 μl of medium was used to measure the absorbance OD value at 570 nm and 600 nm respectively as per the manufacturer's instructions. Culture medium in the absence of cells was used as the background control, and the corrected OD values were used.

To visualize cell viability, cells were stained with Live/Dead viability/cytotoxicity assay kit (Molecular Probes, Eugene, OR, USA) as reported previously [18]. Cells were incubated with calcein AM (2 μM), ethidium homodimer-1 (EthD-1, 4 μM), and Hoechst 33342 for 45 min at 37 °C, then imaged using a Leica SP5 CLSM confocal microscope at days 1,8,16, and 24. Fluorescent confocal image stacks in a range of 100–200 μm were captured. The size and the number distribution of cell clusters were measured using Image J software.

RNA isolation and quantitative real-time PCR

Total RNA was extracted from cells using the RNeasy mini purification kit (Qiagen, Valencia, CA) according to the manufacturer's instructions. For cells in 3D, three hydrogel constructs were pooled and cut into smaller pieces prior to RNA extraction. RNA concentration was quantified using a BioRad SmartSpect3000, and samples with a 260/280 ratio higher than 1.7 were used to prepare cDNA. Single-strand cDNA was synthesized using the TaqMan Reverse Transcription Reagents (Life Technologies). Real-time PCR was performed using the SYBR-Green PCR master mix (Invitrogen) on a Multiplex Quantitative PCR System (STRATAGENE, Model Mx3000pTM) with a final volume of 25 μl for each reaction under the following cycling conditions: 95 °C for 10 min; 95 °C for 15s and 60 °C for 1 min (40 cycles), followed by a dissociation stage. The value of threshold cycle (Ct) was generated at every cycle during a run. Expression of the gene-of-interest was quantitatively analyzed using gene expression analysis software (Bio-rad) [19]. Sequences

of all primers employed in this study were as we reported previously [17]. Gene expression levels were normalized against β-actin for all samples.

Immunofluorescent staining

Hydrogel constructs were washed with PBS and fixed with 100% (v/v) methanol at −20 °C for 10 min. After fixation, constructs were washed with PBS and stored at 4 °C until staining. Constructs were blocked with 500 μl of blocking solution (3% (w/v) BSA with 0.2% (v/v) Triton X-100 in PBS) at room temperature (RT) for 1 h followed by incubation with anti- Ki67 antibody (1:200, Novus Biologicals #9664S), or anti-Cad11 antibody (1:150, zymed, Invitrogen), or anti-CXCR4 antibody (1:400, EMD Millipore, Billerica, MA) at 4 °C overnight. The next day, samples were washed with PBS and incubated with Alexa Fluor 594 or Alexa Fluor 488 (1:400; Jackson ImmunoResearch, Laboratories, INC) at RT for 1 h followed by counterstaining of nuclei with DAPI (5 μg/ml) for 10 min. Samples were washed with PBS and immunofluorescence images were captured with a Leica SP5 CLSM confocal microscope.

Enzyme linked immunosorbent assay (ELISA)

The encapsulated cells (1×10^5/puck) were cultured in wells of 48-well plate with 500 μl of culture medium in each well. The cell culture medium was changed every 2 days and was collected at days 1, 8, 16 and 24. For 2D, cell culture medium was collected on day 4 and normalized with cell number at 1×10^5/ml. The protein levels of vascular endothelial growth factor (VEGF) and receptor activator of nuclear factor kappa-B ligand (RANKL) in cell culture medium were determined using a human VEGF ELISA kit (Life Technologies, KHG0112) and a human RANKL ELISA kit (NEOBIOLAB, #HR0012) respectively, according to the manufacturer's instructions. The absorption OD value was measured at 450 nm.

Statistical analysis

Statistical significance was assessed by Student's *t* test to evaluate the statistical significance between 2D and 3D cultures. The level of significance was set at $p < 0.05$. At least three independent *in vitro* experiments were conducted for all assays and analyses.

Results

Hyaluronic acid (HA)-based hydrogel influences cell morphology, survival and proliferation

Bone-786-O RCC cells cultured on 2D standard tissue culture plastic dish attached and exhibited an extended morphology (Fig. 2a, left). In contrast, when encapsulated within a 3D HA-based hydrogel, bone-786-O RCC cells remained round and formed spheroids (Fig. 2a, right). As described in Methods, bone-786-O RCC cells were obtained from parental 786-O RCC cell transfected with GFP gene as we reported previously, which was also confirmed in this study when bone-786-O RCC cells were cultured in either 2D or 3D culture system (Fig. 2a).

LIVE/DEAD staining revealed that most bone-786-O RCC cells remained viable (stained green) over the 24-day period when cells were encapsulated and cultured in 3D HA-based hydrogels (Fig. 2b). However, when the same number of cells was cultured on 2D in 48-well plates, cells rapidly reached confluence a day after seeding and began to die after day 2 (data not shown). In 3D HA-based hydrogels, multi-cellular spheroids were observed (Fig. 2b) that increased in size over time, reaching an average diameter of 22 μm on day 24 (Fig. 2c). As shown in Fig. 2d, the number of large spheroids also increased from day 1 onwards.

Besides the differences in morphology and enhanced survival observed in bone-786-O RCC cells cultured in 3D HA-based hydrogel, we observed a significantly slower proliferative capacity in 3D-cultured bone-786-O cells as compared to that in 2D using PrestoBlue cell viability assay. The fold increase in viable cell number in 3D was approximately 2–3 folds over day 1 during the 24-day culture. In contrast, a 6–8 fold increase in cell number over day 1 was observed during the 4-day culture in 2D (Fig. 3a). This observation was further corroborated with greater Ki-67-positive cells observed in 2D versus 3D by immunocytochemistry (Fig. 3b).

Expression of adhesion molecules cadherin 11 (Cad11) and CXCR4

Cad11 adhesion molecule has been implicated in kidney bone metastases [17]. Real time PCR analysis revealed that the levels of *Cad11* gene expression in bone-786-O cells were significantly increased in 3D as compared to 2D (Fig. 4a). CXCR4 adhesion molecule has been shown to play a role in advanced and metastatic RCC [20-22]. We asked if changes in culture conditions also affected gene expression of CXCR4. Indeed, *CXCR4* mRNA levels were dramatically increased in bone-786-O cells when cells were cultured in 3D HA-based hydrogel from days 8 to 24 as compared to that observed in 2D cultures (Fig. 4b). Immunofluorescent staining of cells that had been cultured for 8 days in 3D culture showed that levels of Cad11 and CXCR4 proteins were increased compared to that measured in 2D cultures (Fig. 4c,d).

Expression of angiogenic and osteolytic factors

RCC bone metastases are characteristically hypervascular. Several genes for angiogenesis including *HIF-1α*, *VEGF*, and *angiopoeitin-1* (*Ang-1*) were determined on cells cultured in 2D or 3D system by real time PCR. Our results showed that there was no significant difference in the *HIF-1α* mRNA levels between 2D and 3D culture systems (Fig. 5a). However, *VEGF* mRNA was significantly higher in 3D-cultured bone-786-O cells compared with 2D culture (Fig. 5b). *Ang-1* mRNA was also higher in 3D culture (Fig. 5c). Given the osteolytic nature of RCC bone lesions, we also evaluated the expression levels of selected genes including parathyroid hormone-related protein (PTHrP), interleukin 6 (IL-6), and RANKL, all of which are known to play critical roles in modulating bone homeostasis and osteoclastic activity. Both *PTHrP* and *IL-6* mRNA levels were significantly increased in bone-786-O RCC cells in 3D cultures as compared to their counterparts in 2D (Fig. 5d,e). *RANKL* expression was observed primarily in 3D spheroids. In 2D, expression was extremely low (Fig. 5f). However in 3D culture, a dramatic increase in *RANKL* mRNA levels in bone-derived 786-O RCC spheroids was observed after one day, peaking at day 8 (Fig. 5f). Increased VEGF (Fig. 6a) and RANKL (Fig. 6b) protein levels were also detected

in cell culture medium from the 3D system compared to those in 2D. These observations suggest that our model resembles the hyper-vascular and osteolytic characteristics seen in *in vivo*.

Discussion

In this study, we assessed the properties of bone-derived human 786-O RCC cells cultured in a 3D HA-based hydrogel system. We report that bone-derived 786-O RCC cells grow as spheroids in a 3D HA-based hydrogel system with a decreased proliferative capacity as compared to cells cultured on 2D, which grow as a monolayer. The transition from 2D to 3D culture resulted in phenotypic changes that are consistent with the characteristics of RCC bone metastases in patients, such as hypervascularity [23,24] and osteolysis [4,5]. Based on these observations, we conclude that 3D HA-based hydrogels may enable more accurate studies of RCC bone metastasis *in vitro* as compared to traditional 2D models and is a more suitable *in vitro* model for screening drugs for the treatment of bone metastatic RCC.

Similar to previous studies on PCa cells [14,15], bone-derived 786-O RCC cells grown on 2D exhibited a spread-out morphology; whereas cells in 3D grew as multicellular spheroids, containing 10–30 cells. Moreover, the observed slower growth of bone-derived 786-O RCC cells in 3D HA-based hydrogels as compared to the same cells cultured on 2D corroborates previous studies that report a decrease in proliferative capacity when PCa cells are cultured in 3D versus 2D [14,15]. In 3D, PCa cells also adopt a phenotype similar to those of tumor cells growth *in vivo* [25]. It has also been reported that LNCaP PCa cells cultured as multicellular aggregates in HA hydrogel are more resistant to drug treatment, similar to clinical observations [26]. Our *in vitro* 3D HA-based hydrogel model for bone-derived 786-O RCC cells could similarly be beneficial for evaluating novel anti-tumor drugs in future work.

Cad11 adhesion molecule is the major cadherin family protein expressed in osteoblasts, and it has been shown to play a role in prostate cancer [27-29] and breast cancer [15,30] bone metastases. We previously reported that Cad11 expression in human RCC bone metastasis samples is significantly higher than that in primary human RCC tumors [17], implicating a possible role of Cad11 in RCC bone metastasis. CXCR4 has been reported to contribute to metastasis formation in prostate cancer through interacting with its ligand SDF-1 present in the bone marrow [31]. Although *CXCR4* expression can be detected in primary human RCC tumor samples, its expression is higher in advanced or metastatic RCC [20-22]. In this study, we observed increased expression of both *CadH* and *CXCR4* in bone-derived 786-O RCC cells cultured in 3D HA-based hydrogels, suggesting that 3D HA-based hydrogels provide a microenvironment that is more similar to the bone metastatic microenvironment *in vivo*.

RCC bone metastases in patients are characteristically hypervascular, which has been attributed to a common mutation in the gene encoding the von Hippel–Lindau (VHL) E3 ubiquitin ligase that interacts and targets HIF-1α to the proteasome for degradation [32]. Mutation in *VHL* tumor suppressor gene causes the stabilization of HIF-1α and initiates gene transcription of its target genes, leading to up-regulation of several angiogenic factors and growth factors [33-35]. The observed increase in *VEGF* and *Ang1* gene expression and

VEGF protein levels in 3D culture than in 2D suggests that our model is more similar to hypervascularity seen in *in vivo*.

RCC bone metastasis is characterized by severe osteolytic bone lesions, induced by tumor-produced growth factors and/or cytokines, including PTHrP, IL-6, and RANKL, which perturb bone homeostasis by increasing osteoclastic activity [36-38]. It is well documented that PTHrP is highly active in the bone microenvironment where, by activating nearby PTH-responsive cells involved in normal bone turnover, it can trigger bone loss and hypercalcemia [36,39]. In the area immediately around the growing tumor, locally high levels of PTHrP can tip the balance toward resorption, creating a lytic lesion around the tumor [36]. IL-6 has been shown to be produced at high levels in some patients with bone metastatic RCC [40,41]. IL-6 can stimulate osteoclast formation and contribute to mild to severe hypercalcemia [42-44]. RANKL is a type II membrane protein and a member of the tumor necrosis factor (TNF) superfamily. RANKL shed by tumor cells plays a key role in osteoclastic cell differentiation and activation, causing bone resorption [45-48]. RANKL is expressed in both primary and metastatic RCCs and may increase their malignant potential by accelerating the migration of cancer cells and by stimulating osteoclastogenesis [49]. The observed higher expression levels of PTHrP, IL-6 and RANKL in 3D cultured system compared with 2D further support the conclusion that 3D HA-based hydrogel provides an environment that is more similar to tumor *in vivo* for bone-derived RCC cells.

In summary, bone-derived 786-O RCC cells growing in 3D HA-based hydrogels form spheroids that are held together by adhesion molecules common to solid tumors, and express genes that model the *in vivo* characteristics of RCC bone metastasis including those gene products associated with hypervascularity and osteolysis, both qualities that are generally lost in conventional 2D cultures. We propose to use this culture system for further studies to better characterize the phenotype of the RCC spheroids and to determine their suitability for pharmaceutical testing. The 3D model also provides a heretofore unavailable means to study the mechanism of metastasis formation, and for identifying intervention strategies targeting the growth of metastases in bone.

Acknowledgements

This work was supported by the University of Texas MD Anderson Cancer Center (MDACC) Institutional Start-up fund (R. Satcher), MDACC Institutional Research Grant (IRG) Program (R. Satcher), and the NIH P01 CA098912 (M. Farach-Carson).

References

[1]. Amato RJ. Renal cell carcinoma: review of novel single-agent therapeutics and combination regimens. Ann. Oncol. 2005; 16:7–15. [PubMed: 15598929]

[2]. Sourbier C, Massfelder T. Parathyroid hormone-related protein in human renal cell carcinoma. Cancer Lett. 2006; 240:170–182. [PubMed: 16223565]

[3]. Gupta K, Miller JD, Li JZ, Russell MW, Charbonneau C. Epidemiologic and socioeconomic burden of metastatic renal cell carcinoma (mRCC): a literature review. Cancer Treat. Rev. 2008; 34:193–205. [PubMed: 18313224]

[4]. Wood SL, Brown JE. Skeletal metastasis in renal cell carcinoma: current and future management options. Cancer Treat. Rev. 2012; 38:284–291. [PubMed: 21802857]

[5]. Woodward E, Jagdev S, McParland L, Clark K, Gregory W, Newsham A, et al. Skeletal complications and survival in renal cancer patients with bone metastases. Bone. 2011; 48:160–166. [PubMed: 20854942]

[6]. Lee J, Cuddihy MJ, Kotov NA. Three-dimensional cell culture matrices: state of the art. Tissue Eng. Part B Rev. 2008; 14:61–86. [PubMed: 18454635]

[7]. Sasser AK, Mundy BL, Smith KM, Studebaker AW, Axel AE, Haidet AM, et al. Human bone marrow stromal cells enhance breast cancer cell growth rates in a cell line-dependent manner when evaluated in 3D tumor environments. Cancer Lett. 2007; 254:255–264. [PubMed: 17467167]

[8]. Yamada KM, Cukierman E. Modeling tissue morphogenesis and cancer in 3D. Cell. 2007; 130:601–610. [PubMed: 17719539]

[9]. DeVolder R, Kong HJ. Hydrogels for in vivo-like three-dimensional cellular studies. WIREs Syst. Biol. Med. 2012; 4:351–365.

[10]. Alemany-Ribes M, Semino CE. Bioengineering 3D environments for cancer models. Adv. Drug Deliv. Rev. 2014; 79-80:40–49. [PubMed: 24996134]

[11]. Wang R, Xu J, Juliette L, Castilleja A, Love J, Sung SY, et al. Three-dimensional co-culture models to study prostate cancer growth, progression, and metastasis to bone. Semin. Cancer Biol. 2005; 15:353–364. [PubMed: 15982899]

[12]. Windus LC, Glover TT, Avery VM. Bone-stromal cells up-regulate tumourigenic markers in a tumour-stromal 3D model of prostate cancer. Mol. Cancer. 2013; 12:112. [PubMed: 24073816]

[13]. Fong EL, Martinez M, Yang J, Mikos AG, Navone NM, Harrington DA, et al. Hydrogel-based 3D model of patient-derived prostate xenograft tumors suitable for drug screening. Mol. Pharm. 2014; 11:2040–2050. [PubMed: 24779589]

[14]. Gurski LA, Jha AK, Zhang C, Jia X, Farach-Carson MC. Hyaluronic acid-based hydrogels as 3D matrices for in vitro evaluation of chemotherapeutic drugs using poorly adherent prostate cancer cells. Biomaterials. 2009; 30:6076–6085. [PubMed: 19695694]

[15]. Xu X, Gurski LA, Zhang C, Harrington DA, Farach-Carson MC, Jia X. Recreating the tumor microenvironment in a bilayer, hyaluronic acid hydrogel construct for the growth of prostate cancer spheroids. Biomaterials. 2012; 33:9049–9060. [PubMed: 22999468]

[16]. Gurski LA, Xu X, Labrada LN, Nguyen NT, Xiao L, van Golen KL, et al. Hyaluronan (HA) interacting proteins rHaMM and hyaluronidase impact prostate cancer cell behavior and invadopodia formation in 3D HA-based hydrogels. PLoS ONE. 2012; 7:e50075. [PubMed: 23166824]

[17]. Satcher RL, Pan T, Cheng CJ, Lee YC, Lin SC, Yu G, et al. Cadherin-11 in renal cell carcinoma bone metastasis. PLoS ONE. 2014; 9:e89880. [PubMed: 24587095]

[18]. Pan T, Rawal P, Wu Y, Xie W, Jankovic J, Le W. Rapamycin protects against rotenone-induced apoptosis through autophagy induction. Neuroscience. 2009; 164:541–551. [PubMed: 19682553]

[19]. Le W, Pan T, Huang M, Xu P, Xie W, Zhu W, et al. Decreased NURR1 gene expression in patients with Parkinson's disease. J. Neurol. Sci. 2008; 273:29–33. [PubMed: 18684475]

[20]. D'Alterio C, Consales C, Polimeno M, Franco R, Cindolo L, Portella L, et al. Concomitant CXCR4 and CXCR7 expression predicts poor prognosis in renal cancer. Curr. Cancer Drug Targets. 2010; 10:772–781. [PubMed: 20578990]

[21]. Pan J, Mestas J, Burdick MD, Phillips RJ, Thomas GV, Reckamp K, et al. Stromal derived factor-1 (SDF-1/CXCL12) and CXCR4 in renal cell carcinoma metastasis. Mol. Cancer. 2006; 5:56. [PubMed: 17083723]

[22]. Wehler TC, Graf C, Biesterfeld S, Brenner W, Schadt J, Gockel I, et al. Strong expression of chemokine receptor CXCR4 by renal cell carcinoma correlates with advanced disease. J. Oncol. 2008; 2008:626340. [PubMed: 19266088]

[23]. Xie C, Schwarz EM, Sampson ER, Dhillon RS, Li D, O'Keefe RJ, et al. Unique angiogenic and vasculogenic properties of renal cell carcinoma in a xenograft model of bone metastasis are associated with high levels of vegf-a and decreased ang-1 expression. J. Orthop. Res. 2012; 30:325–333. [PubMed: 21809376]

[24]. Yamakawa M, Liu LX, Belanger AJ, Date T, Kuriyama T, Goldberg MA, et al. Expression of angiopoietins in renal epithelial and clear cell carcinoma cells: regulation by hypoxia and

participation in angiogenesis. Am. J. Physiol. Renal Physiol. 2004; 287:F649–F657. [PubMed: 15198927]

[25]. Foster BA, Gingrich JR, Kwon ED, Madias C, Greenberg NM. Characterization of prostatic epithelial cell lines derived from transgenic adenocarcinoma of the mouse prostate (TRAMP) model. Cancer Res. 1997; 57:3325–3330. [PubMed: 9269988]

[26]. Xu X, Sabanayagam CR, Harrington DA, Farach-Carson MC, Jia X. A hydrogel-based tumor model for the evaluation of nanoparticle-based cancer therapeutics. Biomaterials. 2014; 35:3319–3330. [PubMed: 24447463]

[27]. Lee YC, Cheng CJ, Huang M, Bilen MA, Ye X, Navone NM, et al. Androgen depletion up-regulates cadherin-11 expression in prostate cancer. J. Pathol. 2010; 221:68–76. [PubMed: 20191612]

[28]. Huang CF, Lira C, Chu K, Bilen MA, Lee YC, Ye X, et al. Cadherin-11 increases migration and invasion of prostate cancer cells and enhances their interaction with osteoblasts. Cancer Res. 2010; 70:4580–4589. [PubMed: 20484040]

[29]. Chu K, Cheng CJ, Ye X, Lee YC, Zurita AJ, Chen DT, et al. Cadherin-11 promotes the metastasis of prostate cancer cells to bone. Mol. Cancer Res. 2008; 6:1259–1267. [PubMed: 18708358]

[30]. Tamura D, Hiraga T, Myoui A, Yoshikawa H, Yoneda T. Cadherin-11-mediated interactions with bone marrow stromal/osteoblastic cells support selective colonization of breast cancer cells in bone. Int. J. Oncol. 2008; 33:17–24. [PubMed: 18575746]

[31]. Taichman RS, Cooper C, Keller ET, Pienta KJ, Taichman NS, McCauley LK. Use of the stromal cell-derived factor-1/CXCR4 pathway in prostate cancer metastasis to bone. Cancer Res. 2002; 62:1832–1837. [PubMed: 11912162]

[32]. Chan DA, Sutphin PD, Yen SE, Giaccia AJ. Coordinate regulation of the oxygen-dependent degradation domains of hypoxia-inducible factor 1 alpha. Mol. Cell. Biol. 2005; 25:6415–6426. [PubMed: 16024780]

[33]. Wiesener MS, Munchenhagen PM, Berger I, Morgan NV, Roigas J, Schwiertz A, et al. Constitutive activation of hypoxia-inducible genes related to overexpression of hypoxia-inducible factor-1alpha in clear cell renal carcinomas. Cancer Res. 2001; 61:5215–5222. [PubMed: 11431362]

[34]. Blancher C, Moore JW, Robertson N, Harris AL. Effects of ras and von Hippel-Lindau (VHL) gene mutations on hypoxia-inducible factor (HIF)-1alpha, HIF-2alpha, and vascular endothelial growth factor expression and their regulation by the phosphatidylinositol 3'-kinase/Akt signaling pathway. Cancer Res. 2001; 61:7349–7355. [PubMed: 11585776]

[35]. Fukuhara S, Sako K, Noda K, Zhang J, Minami M, Mochizuki N. Angiopoietin-1/Tie2 receptor signaling in vascular quiescence and angiogenesis. Histol. Histopathol. 2010; 25:387–396. [PubMed: 20054809]

[36]. Guise TA, Yin JJ, Thomas RJ, Dallas M, Cui Y, Gillespie MT. Parathyroid hormone-related protein (PTHrP)-(1–139) isoform is efficiently secreted in vitro and enhances breast cancer metastasis to bone in vivo. Bone. 2002; 30:670–676. [PubMed: 11996903]

[37]. Kakonen SM, Mundy GR. Mechanisms of osteolytic bone metastases in breast carcinoma. Cancer. 2003; 97:834–839. [PubMed: 12548583]

[38]. Sottnik JL, Keller ET. Understanding and targeting osteoclastic activity in prostate cancer bone metastases. Curr. Mol. Med. 2013; 13:626–639. [PubMed: 23061677]

[39]. Martin TJ. Osteoblast-derived PTHrP is a physiological regulator of bone formation. J. Clin. Invest. 2005; 115:2322–2324. [PubMed: 16138187]

[40]. Negrier S, Perol D, Menetrier-Caux C, Escudier B, Pallardy M, Ravaud A, et al. Interleukin-6, interleukin-10, and vascular endothelial growth factor in metastatic renal cell carcinoma: prognostic value of interleukin-6 – from the Groupe Francais d'Immunotherapie. J. Clin. Oncol. 2004; 22:2371–2378. [PubMed: 15197198]

[41]. Paule B. [Interleukin-6 and bone metastasis of renal cancer: molecular bases and therapeutic implications]. Prog. Urol. 2001; 11:368–375. [PubMed: 11400511]

[42]. de la Mata J, Uy HL, Guise TA, Story B, Boyce BF, Mundy GR, et al. Interleukin-6 enhances hypercalcemia and bone resorption mediated by parathyroid hormone-related protein in vivo. J. Clin. Invest. 1995; 95:2846–2852. [PubMed: 7769125]

[43]. Grey A, Mitnick MA, Masiukiewicz U, Sun BH, Rudikoff S, Jilka RL, et al. A role for interleukin-6 in parathyroid hormone-induced bone resorption in vivo. Endocrinology. 1999; 140:4683–4690. [PubMed: 10499526]

[44]. Delk NA, Farach-Carson MC. Interleukin-6: a bone marrow stromal cell paracrine signal that induces neuroendocrine differentiation and modulates autophagy in bone metastatic PCa cells. Autophagy. 2012; 8:650–663. [PubMed: 22441019]

[45]. Grimaud E, Soubigou L, Couillaud S, Coipeau P, Moreau A, Passuti N, et al. Receptor activator of nuclear factor kappaB ligand (RANKL)/osteoprotegerin (OPG) ratio is increased in severe osteolysis. Am. J. Pathol. 2003; 163:2021–2031. [PubMed: 14578201]

[46]. Wada T, Nakashima T, Hiroshi N, Penninger JM. RANKL-RANK signaling in osteoclastogenesis and bone disease. Trends Mol. Med. 2006; 12:17–25. [PubMed: 16356770]

[47]. Coleman RE. Metastatic bone disease: clinical features, pathophysiology and treatment strategies. Cancer Treat. Rev. 2001; 27:165–176. [PubMed: 11417967]

[48]. Castellano D, Sepulveda JM, Garcia-Escobar I, Rodriguez-Antolin A, Sundlov A, Cortes-Funes H. The role of RANK-ligand inhibition in cancer: the story of denosumab. Oncologist. 2011; 16:136–145. [PubMed: 21285392]

[49]. Mikami S, Katsube K, Oya M, Ishida M, Kosaka T, Mizuno R, et al. Increased RANKL expression is related to tumour migration and metastasis of renal cell carcinomas. J. Pathol. 2009; 218:530–539. [PubMed: 19455604]

Highlights

- Bone-derived 786-O RCC cells encapsulated and cultured in HA-based hydrogel 3D culture system grow as spheroids with a decreased proliferative capacity as compared to that cultured on 2D.
- The transition from 2D to 3D culture results in phenotypic changes including the expression of genes for hypervascularity and osteolysis, modeling *in vivo* characteristics of *RCC* bone metastasis.
- This established model of RCC bone metastases on HA-based hydrogel 3D culture system enables more accurate studies of RCC bone metastasis *in vitro*.

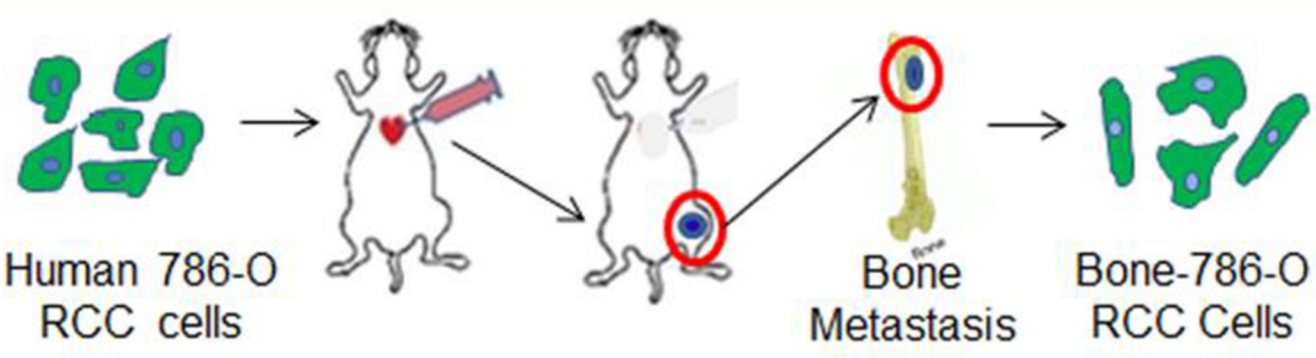

Fig. 1.

Schematic model depicts how the bone-derived human 786-O RCC cells (bone-786-O RCC) were obtained from RCC bone metastases via intra-cardiac injection of mice with human 786-O RCC cells expressing luciferase (Luc) and green fluorescent protein (GFP) genes.

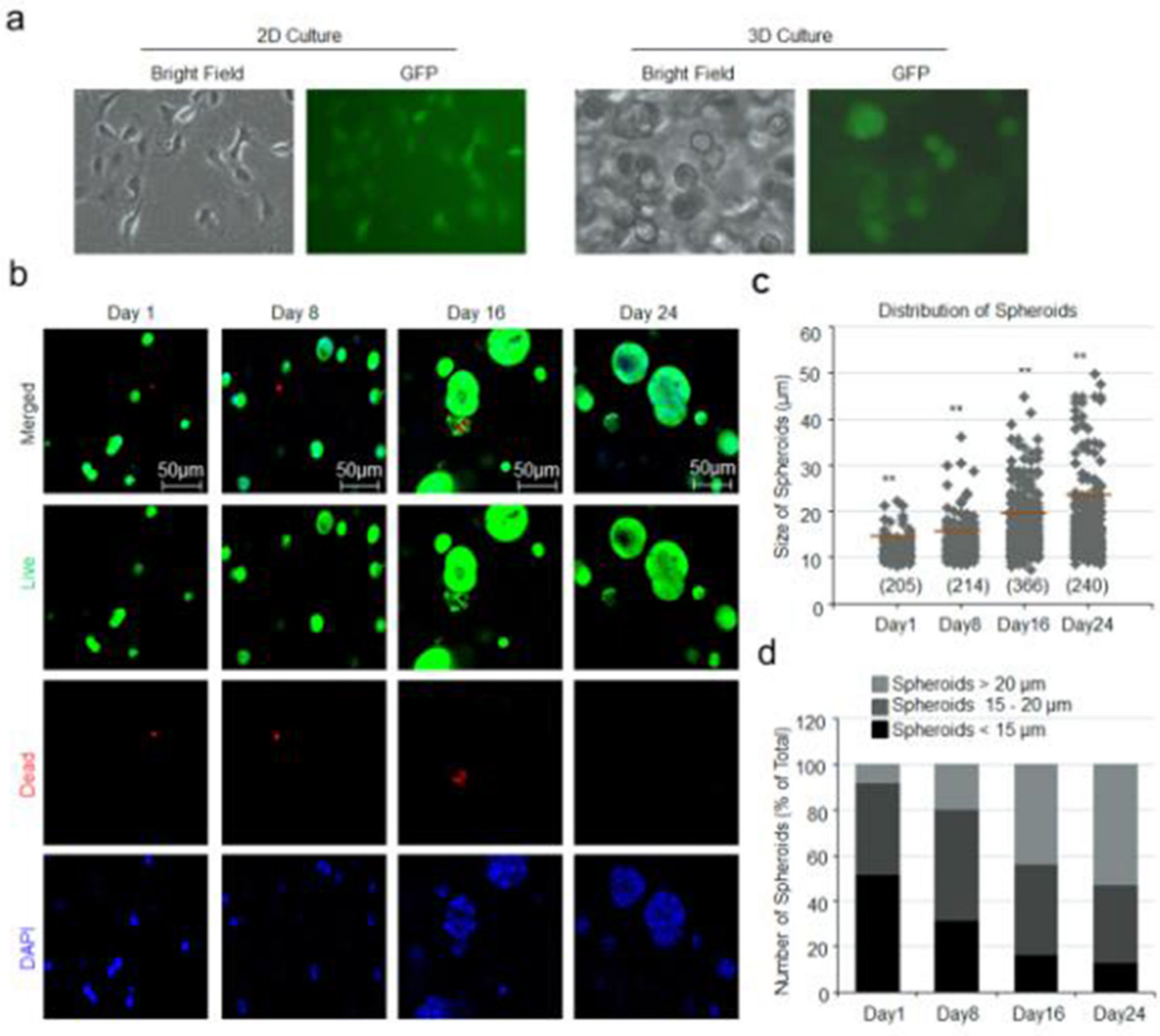

Fig. 2.

Survival of bone-786-O RCC cells in 3D HA-based hydrogel. (a) Morphologies of bone-786-O-RCC cells in two-dimensional (2D) and in three dimensional (3D) culture systems. (b) Encapsulated bone-786-O RCC cells were cultured in HA-based hydrogel for days 1, 8,16 and 24, respectively. Cells were stained with calcein-AM for live cells (green) and ethidium homodimer-1 for dead cells (red). The nuclei were stained with Hoechst (Blue). Magnification = 200× ; Scale bar = 50 μm. (c) Distribution and size of spheroids in 3D HA-based hydrogel. Numbers in parentheses indicate the number of clusters counted. *: $p < 0.05$; **: $p < 0.001$ as compared to day 1. (d) Percentage of various sizes of spheroids formed in HA-based hydrogel over 1, 8, 16 and 24 days. Large, size ≥ 20 μm; Medium, size 15–20 μm; Small, size < 15 μm. (For interpretation of the references to color in this figure legend, the reader is referred to the web version of this article.)

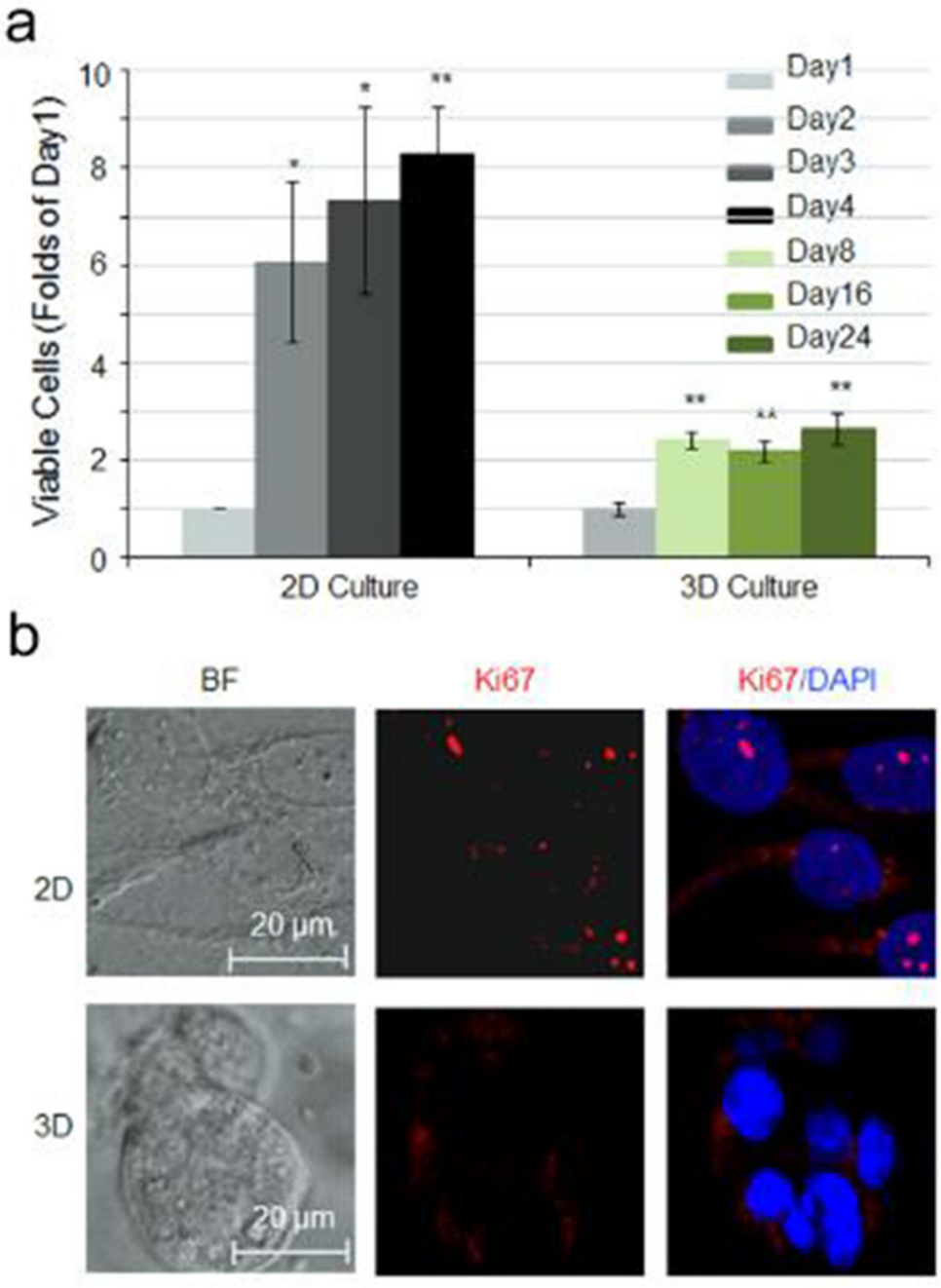

Fig. 3.

Effect of HA-based hydrogel on cell proliferation. (a) Cell viability of bone-786-O RCC cells in 2D culture dishes over 4 days and in 3D HA-based hydrogel over 24 days. Data were expressed as folds of day 1. Values were the mean ± SE. *: $p < 0.05$; **: $p < 0.01$ as compared to day 1. (b) Immunofluorescence staining of cells with anti-Ki67 antibody (red) and DAPI (blue). Magnification = 400× Scale bar = 20 μm. (For interpretation of the references to color in this figure legend, the reader is referred to the web version of this article.)

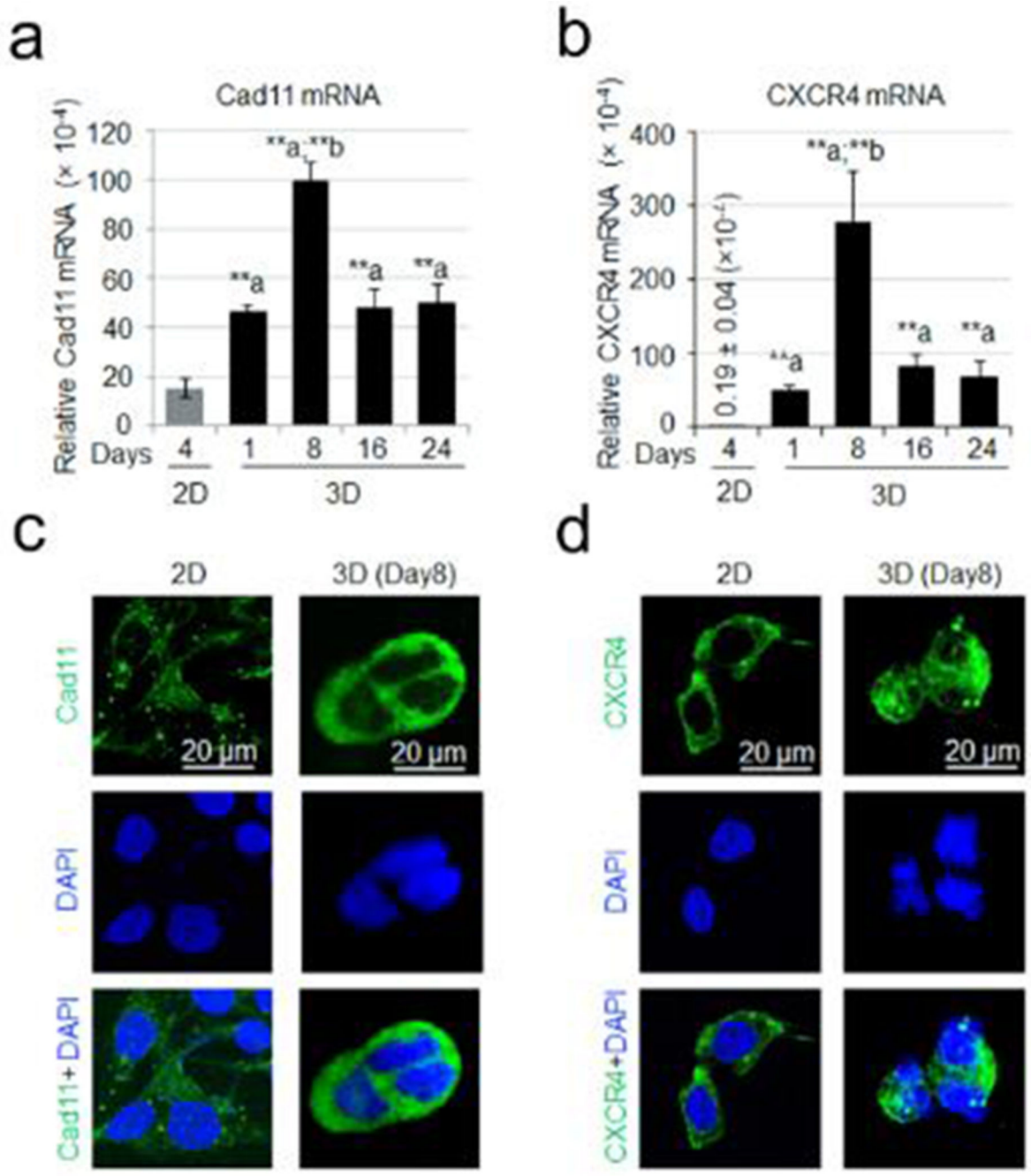

Fig. 4.

Transcripts encoding adhesion molecules. Quantitative PCR was used to measure the message levels encoding adhesion molecules Cad11 (a) and CXCR4 (b). Data were expressed as relative gene expression and the values were the Mean ± S.E. *: $p < 0.05$; **: $p < 0.01$ as compared to 2D. Immunofluorescent staining of Cad11 (c) and CXCR4 (d) showed the relative amount of these proteins in 2D and 3D culture systems.

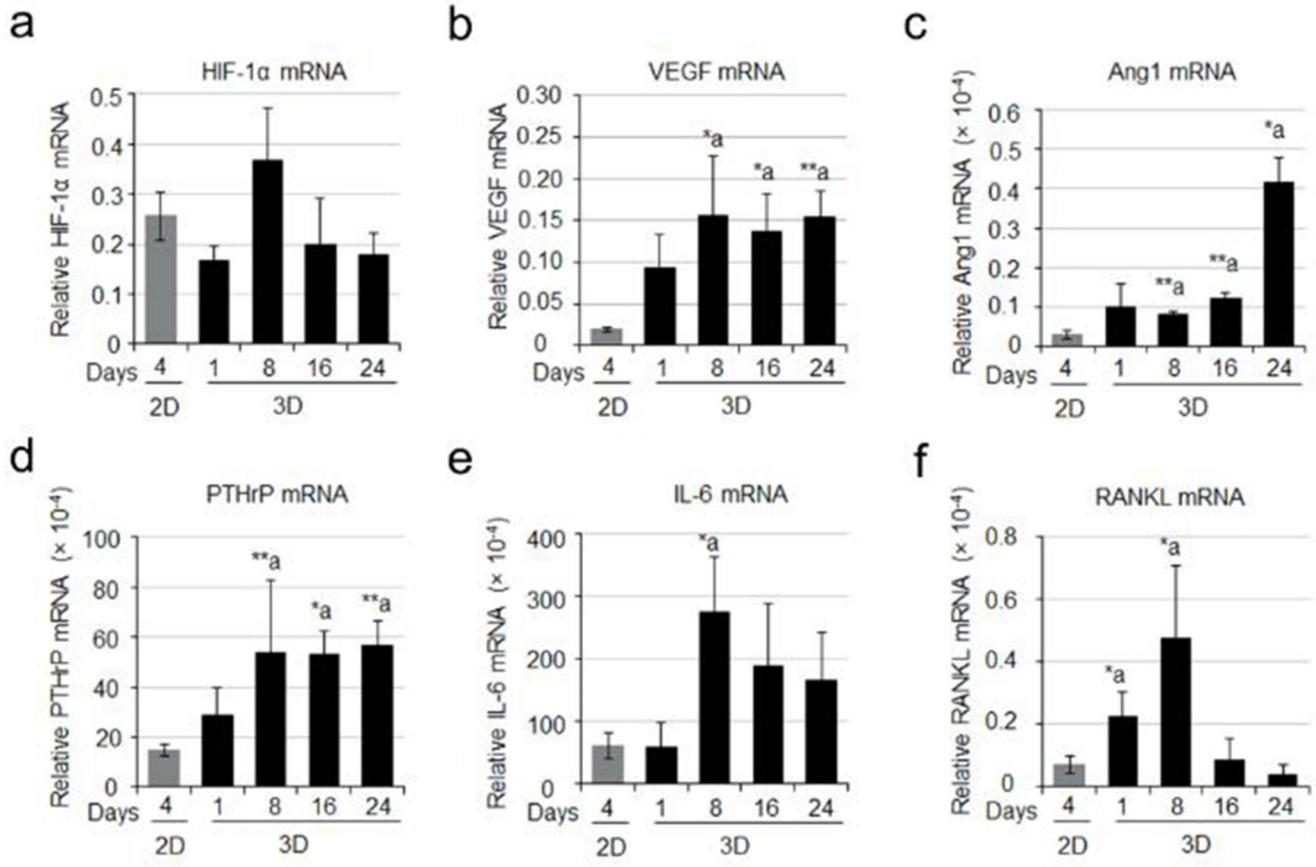

Fig. 5.

Transcripts encoding angiogenic and osteolytic factors. Quantitative PCR was used to measure the message levels encoding angiogenic molecules including HIF-1α (a), VEGF (b) and Ang1 (c), and osteolytic factors including PTHrP (d), IL-6 (e) and RANKL (f). Data were expressed as relative gene expression and the values were the Mean ± S.E. *: $p < 0.05$; **: $p < 0.01$ as compared to 2D.

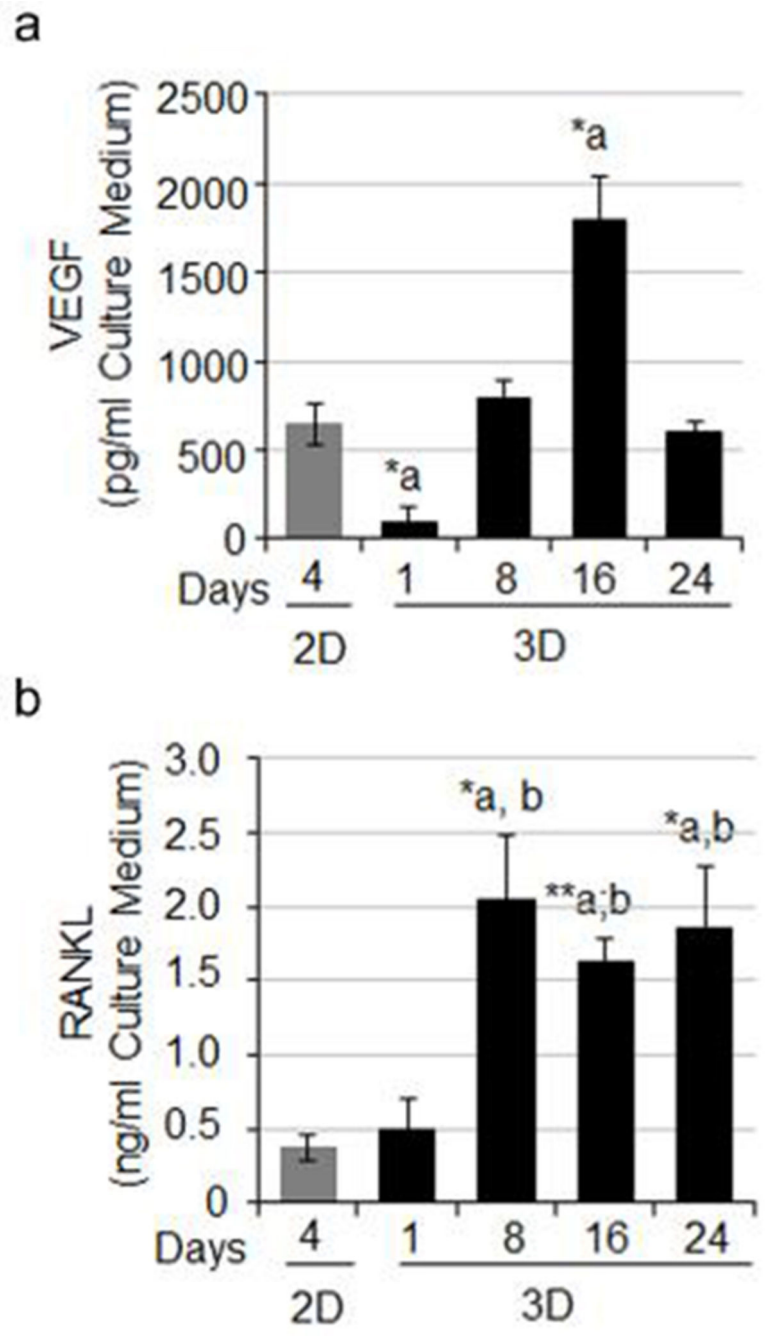

Fig. 6.

Protein expression of VEGF and RANKL. The levels of secreted VEGF protein (a) and RANKL protein (b) each were determined using an ELISA kit and the OD values were measured at 450 nm. The values were the Mean ± S.E. *: $p < 0.05$; **: $p < 0.01$ as compared to 2D.